# Computation of diffusive shock acceleration using stochastic differential equations

**A. Marcowith and J.G. Kirk**

Max-Planck-Institut für Kernphysik, Postfach 10 39 80, D-69029, Heidelberg, Germany

**Abstract.** The present work considers diffusive shock acceleration at non-relativistic shocks using a system of stochastic differential equations (SDE) equivalent to the Fokker-Planck equation. We compute approximate solutions of the transport of cosmic particles at shock fronts with a SDE numerical scheme. Only the first order Fermi process is considered. The momentum gain is given by implicit calculations of the fluid velocity gradients using a linear interpolation between two consecutive time steps. We first validate our procedure in the case of single shock acceleration and retrieve previous analytical derivations of the spectral index for different values of the Péclet number. The spectral steepening effect by synchrotron losses is also reproduced. A comparative discussion of implicit and explicit schemes for different shock thickness shows that implicit calculations extend the range of applicability of SDE schemes to infinitely thin 1D shocks. The method is then applied to multiple shock acceleration that can be relevant for Blazar jets and accretion disks and for galactic centre sources. We only consider a system of identical shocks which free parameters are the distance between two consecutive shocks, the synchrotron losses time and the escape time of the particles. The stationary distribution reproduces quite well the flat differential logarithm energy distribution produced by multiple shock effect, and also the piling-up effect due synchrotron losses at a momentum where they equilibrate the acceleration rate. At higher momenta particle losses dominate and the spectrum drops. The competition between acceleration and loss effects leads to a pile-up shaped distribution which appears to be effective only in a restrict range of inter-shock distances of $\sim$ 10–100 diffusion lengths. We finally compute the optically thin synchrotron spectrum produced such periodic pattern which can explain flat and/or inverted spectra observed in Flat Radio spectrum Quasars and in the galactic centre.

**Key words:** acceleration of particles – shock waves – radiation mechanisms: non-thermal – Galaxy: center – galaxies: BL Lacertae objects: general

---

## 1. Introduction

The non-thermal radio and high-energy radiation spectra from extragalactic and galactic objects such as X-ray binaries, micro-quasars, active galactic nuclei, jets and gamma-ray bursts require the presence of non-thermal particle distributions. One of the prime mechanisms for producing such distributions is diffusive acceleration at a shock front. This theory assumes the particle distributions are isotropised by efficient scattering on wave turbulence on both sides of the shock and gain energy by a first order Fermi process upon crossing it. The equation governing the particle distribution is of the Fokker-Planck type, containing both advection (dynamical friction) and diffusion terms in the spatial variables and an advection term in the energy variable (or in the magnitude of the particle momentum $p$), which is proportional to the divergence of the fluid flow, and remains valid in an integral sense even across shock fronts. Many generalisations of this equation have been discussed, but for the application to non-thermal radiation spectra, the most relevant are the inclusion of synchrotron losses (Webb et al. 1984) and the extension to systems containing multiple shock fronts (Blandford & Ostriker 1980, Spruit 1988, Achterberg 1990, Schneider 1993, Melrose 1996, Melrose & Crouch 1997). However, because of the difficulty of solving the Fokker-Planck equation when the coefficients are complicated (and possibly discontinuous) functions of position, these papers either adopted an idealised situation, or developed approximation schemes valid in only part of the parameter space. A particularly interesting alternative approach is to use the equivalence of the Fokker-Planck equation to a system of stochastic differential equations (SDE's). Numerical integration of these is then akin to a Monte-Carlo simulation of the problem, which is relatively simple to implement, applies to complex flow patterns and places no restriction on the number of phase-space dimensions (e.g., Gardiner 1983). Several conventional Monte-Carlo simulations of particle acceleration exist (for a review see Jones & Ellison 1991), usually assuming a prescribed form of the mean free path of the particle as a function of the particle rigidity and plasma density. They have the advantage of being able to describe the evolution of both the thermal and suprathermal populations, as well as the non-linear back reaction of the non-thermal component on the shock profile. Relativistic shocks and large angle scattering are also

easy to include in such simulations (see Ellison et al. 1990). However, this approach always makes additional assumptions concerning the particle trajectory (e.g., that it is unperturbed between isotropising 'collisions') which go beyond the diffusion approximation. In comparison, the SDE approach adopts the diffusion approximation for test particle and is restricted to the transport of suprathermal particles.

It is only recently that SDE systems have been applied to astrophysical problems: in solar physics with the investigation of acceleration of fast electrons in the solar corona (MacKinnon & Craig 1991, Conway et al. 1998) and in space physics with ion acceleration at the solar termination shock (Chalov et al. 1995). In two papers Achterberg & Krülls (1992) and Krülls & Achterberg (1994 – henceforth KA94), have applied the SDE approach to the problem of particle acceleration at astrophysical shocks, including the possibility of second-order Fermi acceleration (Schlickeiser 1989). These authors drew several important conclusions. In particular, they showed that for Kolmogorov turbulence the second-order acceleration effect is restricted to a small momentum range close to that of injection, because of the increase of the diffusion time with momentum. At high momentum, in contrast, the spectrum is formed by the competing effects of synchrotron losses and the first-order Fermi process.

The numerical scheme used in KA94 is *explicit*, that is, the first-order Fermi acceleration term in the SDE is integrated forwards in time using the value of the fluid velocity gradient at the beginning of each step. This method requires a step short enough to resolve sharp features in the flow, such as a shock transition, and thus severely limits the ability to simulate acceleration in complex flow patterns containing structure on a large range of spatial scales. Our purpose in this paper is to propose and test an *implicit* method of integrating the SDE's. By implicit we mean that the coefficient of the first-order Fermi acceleration term is computed by linear interpolation between the end points of each time step. Such a scheme allows one to treat discontinuous shock structures using a finite time step and thus opens up the prospect of finding approximate numerical solutions of the advection-diffusion equation in complex flow patterns where the gradients of the fluid flow may become large over a distance much shorter than the shock thickness. This is our longer term goal; for the present, we limit ourselves to the problem of a 1D single shock or to systems of multiple shocks.

The organisation of the paper is as follows: in Sect. 2 we present the SDE system equivalent to the advection-diffusion equation and describe the explicit and implicit integration methods. We then test the implicit scheme in Sect. 3 by applying it to the (well-known) problem of acceleration at a single isolated shock front, both with and without synchrotron losses. We also compare the performances of implicit and explicit schemes. Sect. 4 focuses on the application to acceleration in a system of multiple shocks. Here, as well as testing the code against known approximate solutions, we present new solutions valid in regions of parameter space inaccessible to the analytic methods. We use the results to calculate the optically thin synchrotron radiation produced by the stationary particle distribution within a periodic pattern of shocks. In Sect. 5 we summarise our results and discuss extensions of the method to more complex problems.

## 2. Monte-Carlo simulations

### 2.1. Formulation of the SDE's

The usual form of the advection-diffusion equation, describing the transport of cosmic-rays (Skilling 1975) is (in 3D)

$$\frac{\partial f}{\partial t} + (\boldsymbol{u} \cdot \nabla) f - \frac{1}{3} (\nabla \cdot \boldsymbol{u}) p \frac{\partial f}{\partial p} = S + D. \tag{1}$$

where $S$ is a source term and $D$ is a diffusion operator of the form

$$D = \nabla \left( \overline{\overline{\kappa}} \nabla f \right). \tag{2}$$

The diffusion tensor $\overline{\overline{\kappa}}$ describes the spatial transport of particles. Adding the effects of synchrotron losses, and second-order Fermi acceleration one finds

$$D = \nabla \left( \overline{\overline{\kappa}} \nabla f \right) + \frac{1}{p^2} \frac{\partial}{\partial p} \left[ a_2(\boldsymbol{x}, p) p^2 \frac{\partial f}{\partial p} - \right.$$
$$\left. - (\boldsymbol{a}_1(\boldsymbol{x}, p) \cdot \nabla) p^2 f + a_{\mathrm{s}}(\boldsymbol{x}) p^4 f \right]. \tag{3}$$

Here the coefficients $a_1$ and $a_2$ describe the second-order Fermi process and $a_{\mathrm{s}}$ synchrotron losses. Eqs. (1) and (3) give the full advection-diffusion equation of cosmic particles in the diffusion approximation.

The general system of SDEs describing the motion of a point $\boldsymbol{X}$ phase space can be written as:

$$\frac{d\boldsymbol{X}}{dt} = \boldsymbol{A}(\boldsymbol{X}) + \overline{\overline{B}}(\boldsymbol{X}) \frac{d\boldsymbol{W}_{\boldsymbol{X}}}{dt}, \tag{4}$$

where $W_{\boldsymbol{X}}$ is a Wiener process: a stochastic diffusive process used to describe Brownian motion, with a conditional probability which follows a Gaussian distribution. For initial conditions given by $W_{\boldsymbol{X}} = W_{\boldsymbol{X}_0}$ at $t = t_0$, we have at time $t$:

$$\langle W_{\boldsymbol{X}} \rangle = W_{\boldsymbol{X}_0},$$
$$\langle (W_{\boldsymbol{X}} - W_{\boldsymbol{X}_0})^2 \rangle = t - t_0. \tag{5}$$

where $\langle \ \rangle$ means the average value. Itô (1951) has shown that the distribution function describing the stochastic trajectories of the point $\boldsymbol{X}$ obeys the Fokker-Planck equation if the coefficients $\boldsymbol{A}$ and $\overline{\overline{B}}$ are identified with the dynamic friction and diffusion coefficients of this equation. In the case of the Fokker-Planck equation (1), together with (2) or (3), the phase space is four-dimensional, $\boldsymbol{X} = (\boldsymbol{x}, p)$, and expressions for the coefficients $\boldsymbol{A}$ and $\overline{\overline{B}}$ are given by KA94. In this paper we shall restrict ourselves to the case of one space dimension, and include only the terms in Eq. (3) describing spatial diffusion and synchrotron losses, i.e., $a_{1,2} = 0$, so that the phase space is two-dimensional: $\boldsymbol{X} = (x, p)$. Further simplifying to the case where the spatial diffusion coefficient is independent of both position and momentum and the loss rate $a_{\mathrm{s}}$ is independent of position, the set of SDE's (4) reduces to

$$\mathrm{d}x = u\mathrm{d}t + \sqrt{2\kappa}\,\mathrm{d}W_x\,, \tag{6}$$

$$\mathrm{d}\ln(p) = -\left(a_{\mathrm{s}}p + \frac{1}{3}\frac{\mathrm{d}u}{\mathrm{d}x}\right)\mathrm{d}t \tag{7}$$

In this system, $W_x$ is a continuous but non-differentiable process, so that, as written, these equations do not exist in a strictly mathematical sense. To overcome this problem Itô (1951) (see also Gardiner 1983) has defined stochastic differential integrals of the form $\int_t B(X(t),t)dW_X$. Approximate solutions of the system of SDE's can be found by discretizing in time:

$$\Delta x = x_{k+1} - x_k = u(x_k)(t_{k+1} - t_k) + \sqrt{2\kappa} \times$$
$$[W(t_{k+1}) - W(t_k)] \tag{8}$$

$$\ln(p_{k+1}/p_k) = -\left(a_{\mathrm{s}}p_k + \frac{1}{3}\left.\frac{\mathrm{d}u}{\mathrm{d}x}\right|_k\right)(t_{k+1} - t_k) \tag{9}$$

The term in brackets is the increment of the Wiener process, which is proportional to the square root of $t_{k+1} - t_k = \Delta t$:

$$\Delta W = \xi\Delta t^{1/2}\,, \tag{10}$$

where $\xi$ is a Gaussian distributed random number with zero mean and unit variance. This is the so-called *Cauchy-Euler* procedure (Gardiner 1983), as used by KA94. At each time step $\Delta t$, the change in $x$ is made up of two parts: an advective (and deterministic) step

$$\Delta x_{\mathrm{adv}} = u(x_k)\Delta t \tag{11}$$

and a diffusive (stochastic) step

$$\Delta x_{\mathrm{diff}} = \xi\sqrt{2\kappa\Delta t}\,. \tag{12}$$

The approximate solutions converge to the exact solution of the SDE for $\Delta t \to 0$. However, this scheme has the disadvantage that $\Delta t$ must be small enough to resolve the spatial structure in $u(x)$. Denoting by $x_{\mathrm{shock}}$ the shortest lengthscale associated with $u(x)$, KA94 found for a particular example the requirement

$$\Delta x_{\mathrm{adv}} \ll \mathrm{Min}\,(\Delta x_{\mathrm{diff}}, x_{\mathrm{shock}}) \tag{13}$$

Thus, although the diffusive step can be long compared to $x_{\mathrm{shock}}$, the advective step must resolve it, and the method is not appropriate for flow patterns containing sharp gradients (or discontinuities).

### 2.2. Implicit Euler schemes

Implicit methods, in which the increments are expressed not just in terms of the solution at the start of a time step, but implicitly in terms of the solution at the end of it, are frequently effective in relieving time-step problems, and have been discussed for SDE's by Smith & Gardiner (1989). Their main advantage is that they yield stable algorithms. However, the problem raised by the condition (13) is not one of instability, but accuracy. Furthermore, it would appear that the advective, deterministic term is more sensitive to the problem than is the diffusive term. In view of this, we have chosen to test an algorithm in which, for the advective term, the coefficient is evaluated neither at

the initial point of a time step (explicit) nor at the end point (fully implicit) but is integrated exactly over the step, using a linear interpolation of the trajectory. In this way, we may hope to account approximately for changes in the velocity $u(x)$ which occur on very small length scales, unresolved by either $\Delta x_{\mathrm{adv}}$, or $\Delta x_{\mathrm{diff}}$.

Replacing the advective terms in Eqs. (8) and (9) using

$$x = \frac{\Delta x}{\Delta t}t \tag{14}$$

we find, neglecting for the moment the synchrotron losses,

$$\Delta x = \int_{t_k}^{t_{k+1}} \mathrm{d}t\, u(x) + \sqrt{2\kappa}\,[W(t_{k+1}) - W(t_k)]$$
$$= \frac{\Delta t}{\Delta x}\int_{x_k}^{x_{k+1}} \mathrm{d}x\, u(x)$$
$$+ \sqrt{2\kappa}\,[W(t_{k+1}) - W(t_k)] \tag{15}$$

$$\ln\left(\frac{p_{k+1}}{p_k}\right) = -\frac{1}{3}\int_{t_k}^{t_{k+1}} \mathrm{d}t\frac{\mathrm{d}u}{\mathrm{d}x}$$
$$= -\frac{\Delta t}{3\Delta x}\,[u(x_{k+1}) - u(x_k)]\,, \tag{16}$$

which has the character of an implicit scheme, since the right-hand side of Eq. (15) is a function of $x_{k+1}$. This technique has been used in applications of SDE to other fields (see Klöden & Platen 1992), but we are not aware of a detailed discussion of its properties. We show in the following that for the test cases we have examined, the scheme yields accurate results when the condition (13) is replaced by the less restrictive one:

$$\Delta x_{\mathrm{adv}} \ll \Delta x_{\mathrm{diff}} \tag{17}$$

## 3. The test case of acceleration at a single shock

We consider an infinite 1D plasma in which particles propagate with diffusion coefficient $\kappa_{\mathrm{D}}$. The flow velocity of the plasma is constant for $x < -x_{\mathrm{shock}}/2$ (the upstream region) and equal to $u_1$ in the shock restframe. Similarly, in the downstream region, $x > x_{\mathrm{shock}}/2$, the velocity is constant, $u_2 = u_1/r$, where $r$ is the compression ratio of the shock. Position, time and momentum are normalised to the diffusion length and time scales upstream: ($\kappa_{\mathrm{D}}/u_1$, and $\kappa_{\mathrm{D}}/u_1^2$ respectively) and the injection momentum of a particle $p_{\mathrm{i}}$. Thus we define the following dimensionless variables and coefficients:

$$\tilde{x} = xu_1/\kappa_{\mathrm{D}}$$
$$\tilde{p} = p/p_{\mathrm{i}}$$
$$\tilde{t} = tu_1^2/\kappa_{\mathrm{D}}$$
$$\tilde{u} = u/u_1$$
$$\tilde{a}_{\mathrm{s}} = a_{\mathrm{s}}(x)/a_{\mathrm{s,0}}$$
$$\eta = u_1\int_{-x_{\mathrm{shock}}/2}^{x_{\mathrm{shock}}/2} \mathrm{d}x/\kappa_{\mathrm{D}}$$
$$= u_1 x_{\mathrm{shock}}/\kappa_{\mathrm{D}} \tag{18}$$

where $a_{\mathrm{s,0}} = 3u_1^2/(2\kappa_{\mathrm{D}}p_i)$ controls the synchrotron losses, and $\eta$ is the Péclet number, since the shock transition is confined to the region $|\tilde{x}| < \eta/2$.
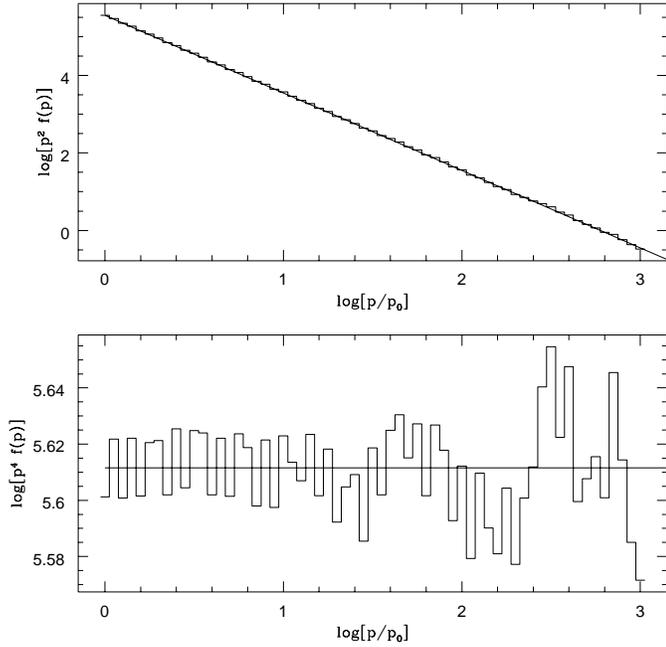
**Fig. 1.** Single shock stationary solution. The parameters are: compression ratio $r = 4$, maximum trajectory time $\tilde{t}_{max} = 3000$, boundaries $L = \pm 1000$, time step $\Delta \tilde{t} = 10^{-3}$. The $x$ step is calculated implicitly using (15). *Upper panel*: comparison between numerical distribution and the analytic solution $f \propto \tilde{p}^{-4}$ (solid line). *Lower panel*: the distribution weighted with $\tilde{p}^4$.

Using the scheme (15,16) we have simulated trajectories in shocks of different $\eta$. Each simulation runs with a given number of particles $N$, injected at momentum $\tilde{p} = 1$, for a given computation time $\tilde{t}_{max}$. Particles can escape at $\tilde{t} < \tilde{t}_{max}$ by crossing a boundary at $|\tilde{x}| = L \gg 1$. The particle distribution is measured at the shock front. Each crossing with an initial momentum $\tilde{p} \geq 1$ increases by unity the differential logarithmic distribution in the bin of momentum bracketing $\tilde{p}$.

It is easily seen from Eq. (16) that for $\eta \ll 1$ large values of $\Delta \ln \tilde{p}$ occur if the advective and diffusive steps almost cancel: $\Delta \tilde{x}_{\mathrm{adv}} \approx -\Delta \tilde{x}_{\mathrm{diff}}$. In this case the result is particularly sensitive to our assumption that the trajectory between the points $\tilde{x}_k$ and $\tilde{x}_{k+1}$ can be interpolated linearly. A partial solution to this problem is to reduce the time step which automatically decreases the probability of choosing a diffusive step which cancels the advective step. However, this procedure increases the computation time. The problem can be avoided completely by replacing the Wiener process by a different random process possessing the same mean and variance, but which effectively prevents the rare steps with $\Delta \tilde{x}_{\mathrm{adv}} \approx -\Delta \tilde{x}_{\mathrm{diff}}$. For a large number of trials, the random step produced by any such distribution tends to the Gaussian form of $W$. The simplest choice is to take $\xi = \pm 1$ with equal probability for each sign.

We first test this prescription in the most difficult case of infinitely thin shocks where $\eta = 0$, in which case the profile shows a discontinuous change in velocity between the up and downstream regions.
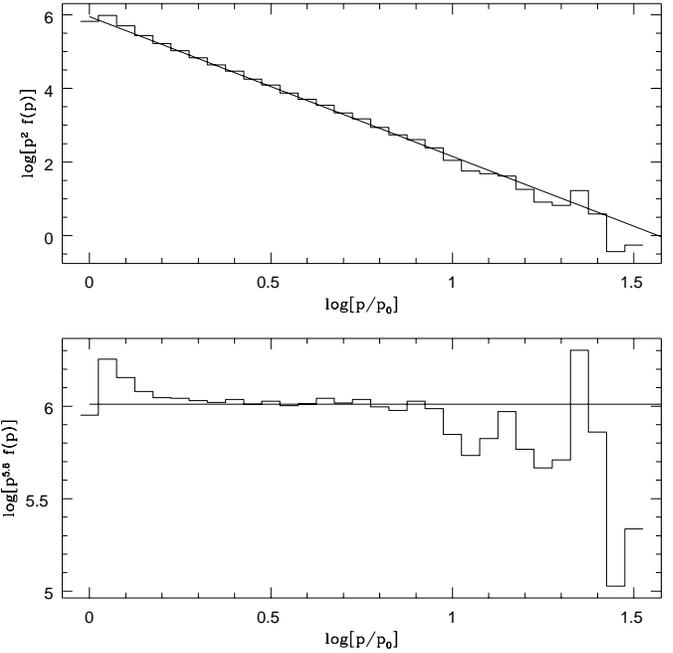


**Fig. 2.** *Upper panel*: the distribution for same parameters as in Fig. 1, but with the Péclet number $\eta = 10$ and time step $\Delta \tilde{t} = 10^{-3}$, compared to the analytical solution $f \propto \tilde{p}^{-5.8}$. *Lower panel*: the spectrum for single shock weighted by $\tilde{p}^{5.8}$.

Fig. 1 gives the stationary spectrum obtained with the modified scheme described above. We found over at least two decades of energy a stationary power-law distribution function of index $s = 3r/(r - 1) = 4$ in the case of strong shocks. Larger computation times are needed to reach the same accuracy at larger momentum. A $\chi^2$ test against the analytic solution gives a value $\sim 1$.

We consider now the case of a shock with Péclet number $\eta \geq 1$. We compare our results with the semi-analytical derivation of the spectral index by Schneider & Kirk (1987). The simulations here use a linear velocity profile

$$\tilde{u}(\tilde{x}) = \frac{1 + r}{2r} - \frac{(r - 1)\tilde{x}}{\eta r} \tag{19}$$

For larger Péclet number, the particles experience a smaller velocity jump at each step. The Fermi process is thus less efficient, leading to softer stationary distributions. For a Péclet number of $\eta = 10$ we get an index of $\sim 5.8$ (see Fig. 2) in good agreements with the results of Schneider & Kirk (1987). The discrepancies seen at small momenta are not statistical errors, but arise because our method assumes zero particle flux in space at the injection point, whereas the scale-independent power-law distribution implies a finite diffusive flux. This 'transient' effect disappears at momenta slightly above that of injection.

### 3.1. Synchrotron losses

Synchrotron losses in the diffusive shock acceleration process have been investigated analytically by Webb et al. (1984). Their main effect is to soften the spectrum at momenta greater than $\tilde{p}_*$

where the loss rate equals the acceleration rate. The inclusion of loss terms in the scheme modifies the way the momentum gain is calculated. Returning to Eq. (7), and using the linear interpolation of the trajectory (14) we arrive at the ordinary differential equation

$$\frac{d\tilde{p}}{d\tilde{x}} = -\tilde{a}_{\mathrm{s}}p^2 \frac{\Delta \tilde{t}}{\Delta \tilde{x}} - \frac{1}{3}\frac{\mathrm{d}\tilde{u}}{\mathrm{d}\tilde{x}}\frac{\Delta \tilde{t}}{\Delta \tilde{x}}\tilde{p}. \tag{20}$$

For the initial condition $\tilde{p} = \tilde{p}_k$ at $\tilde{x} = \tilde{x}_k$ (i.e., $\tilde{t} = \tilde{t}_k$) the solution is

$$\ln\left(\tilde{p}/\tilde{p}_k\right) = -\ln\left(F_{\mathrm{I}} + L_{\mathrm{s}}\right), \tag{21}$$

where the first-order Fermi term ($F_{\mathrm{I}}$) and the loss term $L_{\mathrm{s}}$ are

$$F_{\mathrm{I}} = \exp\left(\frac{\Delta \tilde{u}}{3\Delta \tilde{x}}\Delta \tilde{t}\right), \tag{22}$$

and

$$L_{\mathrm{s}} = \tilde{a}_{\mathrm{s}}\frac{\Delta \tilde{t}}{\Delta \tilde{x}}\tilde{p}_k \int_{\tilde{x}_k}^{\tilde{x}} \exp\left(-\frac{\Delta \tilde{u}}{3\Delta \tilde{x}}\Delta \tilde{t}\right) \mathrm{d}\tilde{x}'. \tag{23}$$

This solution is exact for the linearly interpolated trajectory (14). Having determined $\tilde{x}_{k+1}$ from Eq. (15), the new value of the momentum is given by Eq. (21) with $\tilde{x} = \tilde{x}_{k+1}$.

In Fig. 3, we show the results of this implicit scheme. Following Webb et al. (1984) and KA94, we define upstream and downstream synchrotron coefficients ($a_{\mathrm{s1,s2}}$), given by $a_{\mathrm{s}i} = \tilde{u}^2/(4\tilde{\kappa}\tilde{a}_s\tilde{p}_{\mathrm{i}})$. This gives for the characteristic momentum $\tilde{p}_* = 4/(q/a_{\mathrm{s1}} + (q-3)/a_{\mathrm{s2}})$, with $q = 3r/(r-1)$. For a compression ratio $r = 4$, we have $a_{s1} = 10$ and $a_{s2} = 1$, and the distribution cuts-off for $\tilde{p} > \tilde{p}_* = 2.9$ (i.e., $\log(\tilde{p}) > 0.46$). The solution showed in Fig. 3 is in good agreement with the analytical result of Webb et al. (1984).

The implicit scheme is, of course, much faster than the explicit scheme for flows with small Péclet numbers, since the latter are accurate only when $\Delta \tilde{t} \ll \eta$, whereas for the former $\Delta \tilde{t} \ll 1$ suffices (see Table 1). However, it is also interesting to compare the implicit and explicit schemes in flows with large Péclet numbers, where both should be accurate. In this case, the explicit and implicit schemes give similar results for single shocks for $\Delta \tilde{t} \sim 10^{-3}-10^{-2}$. For larger time steps the particles tend to be advected prematurely from the acceleration zone and both schemes show an unphysical softening of the spectrum. For a given $\Delta \tilde{t}$, the explicit scheme is faster by a factor $\sim 5/3$, since all quantities entering into the computation of the position and momentum increments are calculated only once per time step.

## 4. Acceleration at multiple shocks

The subject of multiple shock acceleration has been extensively investigated both analytically and numerically over the past few years (Spruit 1988, Achterberg 1990, Schneider 1993, Pope & Melrose 1993, Melrose & Crouch 1997). Analytic solutions of the diffusion-advection equation including synchrotron losses can be derived if we assume that the time spent by a fluid element
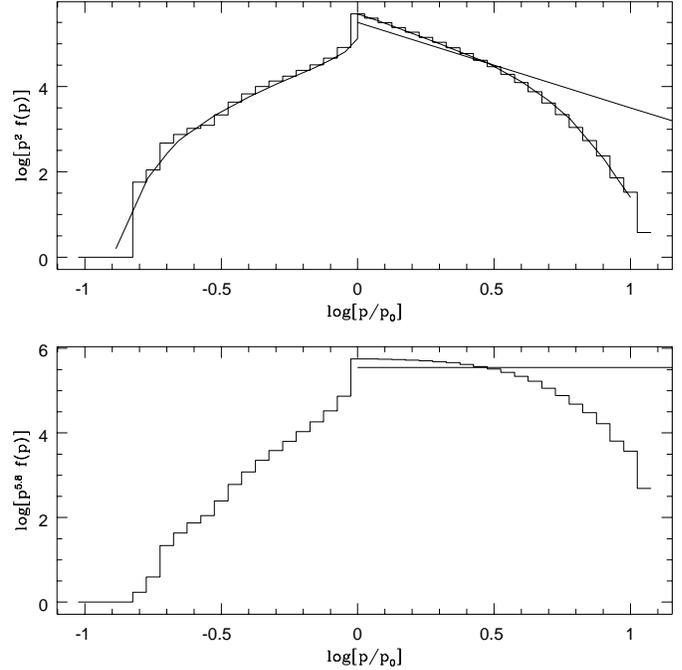


**Fig. 3.** *Upper panel*: the distribution for acceleration at a single shock front including synchrotron losses for $a_{s1} = 10$, $a_{s2} = 1$ and $r = 4$. The thin solid line is adapted from the analytical solution given by Webb et al. (1984). The maximum time for a single trajectory is $\tilde{t}_{max} = 3000$, and $\Delta \tilde{t} = 10^{-3}$. *Lower panel*: the distribution weighted by $\tilde{p}^4$. In each case, the solid line corresponds to the loss free solution.

**Table 1.** Summary of the results of the explicit and implicit schemes. The power-law index of the distribution is compared with the value given by an analytic calculation (Schneider & Kirk 1987).The typical error on the index estimates is of order of $\sim$ few%.

| $\eta$ | Analytic | $\Delta \tilde{t}$ | implicit | explicit |
|---|---|---|---|---|
| $10^{-12}$ | $s = 4.0$ | $10^{-3}$ | s=4.0 | – |
| $210^{-3}$ | $s = 4.0$ | $10^{-3}$ | s=4.01 | s=3.98 |
| $210^{-3}$ | $s = 4.0$ | $10^{-2}$ | s=3.99 | s=4.55 |
| $210^{-3}$ | $s = 4.0$ | $10^{-1}$ | s=4.04 | – |
| 1 | $s = 4.18$ | $10^{-3}$ | s=4.18 | s=4.19 |
| 1 | $s = 4.18$ | $10^{-2}$ | s=4.18 | s=4.19 |
| 1 | $s = 4.18$ | $10^{-1}$ | s=4.21 | s=4.21 |
| 10 | $s = 5.80$ | $10^{-3}$ | s=5.80 | s=5.79 |
| 10 | $s = 5.80$ | $10^{-2}$ | s=5.81 | s=5.82 |
| 10 | $s = 5.80$ | $10^{-1}$ | s=5.85 | s=5.92 |

between two consecutive shocks is much longer than the acceleration time at a single shock problem (see Schneider 1993). Another way of formulating this condition is that the first-order Fermi acceleration process should be much faster than all other processes, such as escape, decompression and losses. With this hypothesis, a final power-law index can be calculated which takes account of the different generations of particles accelerated at individual shocks. At sufficiently high momentum, this approximation fails, since the time-scale of the losses must eventually become comparable to the acceleration time-scale. The effect of multiple shocks is to increase the acceleration ef-

ficiency, by reducing the effective escape rate. In a purely 1D system, the escape rate is formally zero, and the distribution functions tends to $f \propto p^{-3}$. As shown, using spatially averaged equations, by Kardashev (1962) and by Schlickeiser (1984), in the presence of losses, this spectrum extends up to momentum values where the loss effect becomes dominant, and the spectrum piles up at a momentum where the effective acceleration time equals the loss time. More recently, Protheroe & Stanev (1999) (see, however, Drury et al. 1999) have proposed an alternative method of computing the cut-off and pile-up effects in the high energy particle spectrum with various energy dependent diffusion coefficients. They present both an analytical model and a conventional Monte-Carlo simulation (of the same kind as described in the introduction) and show that the effect of the Klein-Nishina regime of inverse Compton losses may modify the results obtained with continuous (synchrotron and inverse Compton in the Thomson regime) losses. In this paper we include neither non-continuous energy losses nor energy dependent diffusion, but postpone an investigation of these effects to future work.

In general for multiple shock system, the picture is somewhat more complicated than depicted in previous analytical or semi-analytical models, since the shocks may be so close together that the acceleration time at a single shock is not short compared to the flow time between the shocks. Also, at high momenta, the synchrotron loss time-scale must be compared not only to the acceleration time at a single shock, but also to the flow time between the shocks.

To investigate these situations, we consider a simple periodic pattern (of period $L$) including shock fronts and re-expansion regions (see Fig. 4). The flow speed of the pattern ($\tilde{x} \in [-L/2, L/2]$) can then be written as

$$\tilde{u}(x) = \tilde{u}_1 + (\tilde{u}_1 - \tilde{u}_2)\frac{\tilde{x} + x_s/2}{L - x_s}, \tilde{x} \in [-L/2, -x_s/2],$$

$$\tilde{u}(x) = \tilde{u}_1 - (\tilde{u}_1 - \tilde{u}_2)\frac{\tilde{x} + x_s/2}{x_s}, \tilde{x} \in [-x_s/2, x_s/2],$$

$$\tilde{u}(x) = \tilde{u}_2 + (\tilde{u}_1 - \tilde{u}_2)\frac{\tilde{x} - x_s/2}{L - x_s}, \tilde{x} \in [x_s/2, L/2] \quad (24)$$

where $\tilde{u}_2 = \tilde{u}_1/r$ is the flow speed on the downstream side of the shock.

There are two free parameters (for a given compression ratio) in this problem: the *advection time* $\tilde{t}_{adv}$, which is the (dimensionless) time for the fluid to flow through one wavelength of the pattern and is numerically equal to the dimensionless length $L$, and the *loss strength* given by $\tilde{a}_s$, which effectively defines a momentum scale, since the (dimensionless) synchrotron loss time at momentum $\tilde{p}$ is

$$\tilde{t}_{syn} = \frac{2}{3\tilde{a}_s \tilde{p}} \quad (25)$$

To these we add a third: an *escape time* $\tilde{t}_{esc}$, assumed independent of $x$ and $p$. This can be understood as a crude way of incorporating 2 or 3-dimensional effects into our 1-dimensional simulation, since only in 1 dimension are the particles unable to
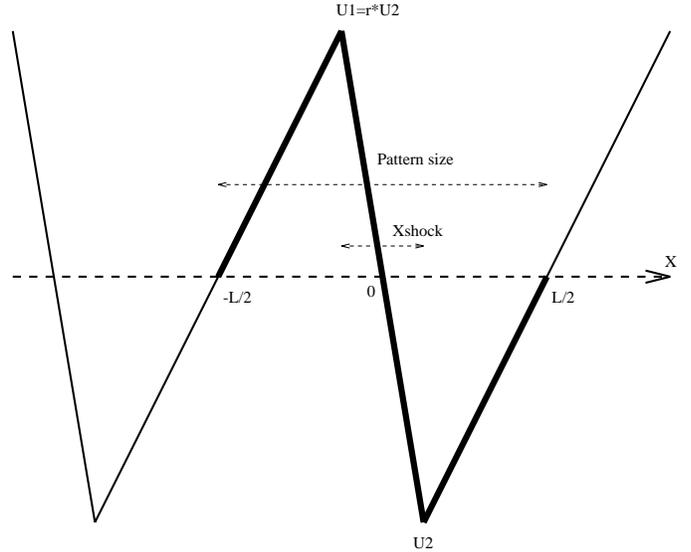


**Fig. 4.** Geometry of the multiple shock system – a single period of the pattern is drawn in bold.

leave the train of shock fronts. The inclusion of escape effects in the SDE system can be effected by rescaling the number of particles that have crossed the shock with at time $\tilde{t}$ by the factor $\exp(-\tilde{t}/\tilde{t}_{esc})$.

There are then two important characteristic times which are important for a discussion of the solutions:

– the single shock acceleration time $\tilde{t}_S$, which is the characteristic time of momentum increase at an isolated shock front:

$$\tilde{t}_S = 3r\frac{1+r}{r-1}, \quad (26)$$

(Lagage & Cesarsky 1981) with $\tilde{\kappa} = \tilde{\kappa}_1 = \tilde{\kappa}_2 = 1$

– the effective multiple shock acceleration time $\tilde{t}_M$ which is controlled by both the advective time and the single shock acceleration time and is inferred from our numerical results.

We present, in the following, results for a shock system described by Eq. (24) with a Péclet number $\eta = 0$. We adopt as typical values of the parameters: compression ratio $r = 4$, escape time $\tilde{t}_{esc} = 10^3$, an inter-shock distance $L = 20$, and, in the case of synchrotron losses, $\tilde{a}_s = 6.5 \times 10^{-6}$ (chosen to give a peak momentum of $10^3$). All the simulations are run for a time of $\tilde{t}_{max} = 5\tilde{t}_{esc}$ and with a time step $\Delta\tilde{t} = 10^{-2}$.

### 4.1. Multiple shock effect: the case without losses

We first consider the case where losses are inefficient ($\tilde{a}_s \to 0$). The results are shown in Fig. 5a. The stationary solution at each shock front $f(x = nL, p)$ (with $n$ an integer) is close to $p^{-3}$. This confirms the multiple shock effect as an efficient way of producing higher energy particles and harder spectra than isolated shocks. In fact, the stationary index is not exactly 3 but slightly steeper, owing to the finite escape time. Using the general relation between the power-law index of accelerated

particles and the escape and acceleration times: $f \propto p^{-s}$, with $s = 3 + \tilde{t}_{\mathrm{acc}}/\tilde{t}_{\mathrm{esc}}$ (Kirk et al. 1994) we find for the effective acceleration time in this particular multiple shock system $\tilde{t}_{\mathrm{M}} \approx 10^2$. Thus, $\tilde{t}_{\mathrm{M}}$ is ($\equiv L$) in this case.

For momenta lower than that of injection, $\tilde{p} \leq 1$, the method of Schneider (1993), and Melrose & Crouch (1997), gives a continuation of the power-law down to $p \sim 1/r$. This is clearly an artifact of the assumed separation of the acceleration and expansion processes. It does not appear in our simulations, which show instead a hardening to lower frequencies starting at the point $\tilde{p} = 1$. However, because of the transients associated with our method close to the injection momentum, this effect may also be an artifact.

At still lower momentum values, the analytical solution $f(p) \propto p^\lambda$ for an escape probability independent of momentum is given by (see Eq. 4.5 in Schneider 1993)

$$\frac{(3r/(r-1)-3)(r^{1+\lambda/3})}{3r/(r-1)+\lambda} = 1 + \frac{\tilde{t}_{\mathrm{adv}}}{\tilde{t}_{\mathrm{esc}}} . \tag{27}$$

The stationary index is $\lambda = 0$ for $\tilde{t}_{\mathrm{esc}} \gg \tilde{t}_{\mathrm{adv}}$, but for lower values of the ratio of escape to multiple shock acceleration time, the spectrum hardens, and typically for a ratio $\tilde{t}_{\mathrm{adv}}/\tilde{t}_{\mathrm{esc}} \sim 0.1$, we get $\lambda \sim 0.2$, in good agreement (given the accuracy of the time-scales) with the simulations; for $p \leq 1$ $f(p) \sim p^{0.3}$ down to $p = 0.1$.

### 4.1.1. Variations of the escape time

If the inter-shock distance $L$ is kept constant, increasing (decreasing) the escape time leads to a harder (softer) stationary spectra. This is clearly seen in Fig. 5b where we have reduced the escape time by a factor of 2 compared to the fiducial case of Fig. 5. The resulting spectrum has an index of 3.2, which again gives $\tilde{t}_{\mathrm{M}} = \mathrm{few} x \tilde{t}_{\mathrm{adv}}$. For momentum $\tilde{p} \leq 1$, from Eq. (27), the relation $\tilde{t}_{\mathrm{esc}} \sim 5\tilde{t}_{\mathrm{M}}$ gives a spectrum with $\lambda \sim 0.4$. We obtained down to $\tilde{p} = 0.1$ an index of $\approx 0.5$. If $\tilde{t}_{\mathrm{esc}} \leq \tilde{t}_{\mathrm{adv}}$, the particles escape the system before being advected to the next shock. The stationary solution tends to the single shock result of Sect. 2.1 without losses, which is a power-law spectrum with an index of 4 (for $r = 4$).

### 4.1.2. Variations of the inter-shock distance

We now keep $\tilde{t}_{\mathrm{esc}}$ constant and equal to the fiducial value of 100. For intershock distances $L \equiv \tilde{t}_{\mathrm{adv}} \gg 100$, no multiple shock effect is seen (Fig. 5c). As in the case of short escape time (Fig. 5b), the stationary solution tends to that from a single shock. As $\tilde{t}_{\mathrm{adv}}$ decreases, the spectrum hardens and the spectral index can take all values between 3 and 4 (for $r = 4$). This is consistent with our finding that $\tilde{t}_{\mathrm{M}} \approx \mathrm{few} \times \tilde{t}_{\mathrm{adv}}$. If the inter-shock distance is reduced to below one diffusion length $L < 1$, the assumptions normally used to derive the basic transport equation (Skilling 1975) are violated. We have not investigated this regime; although it potentially interesting, since if the distribution remains almost isotropic, the diffusion approximation
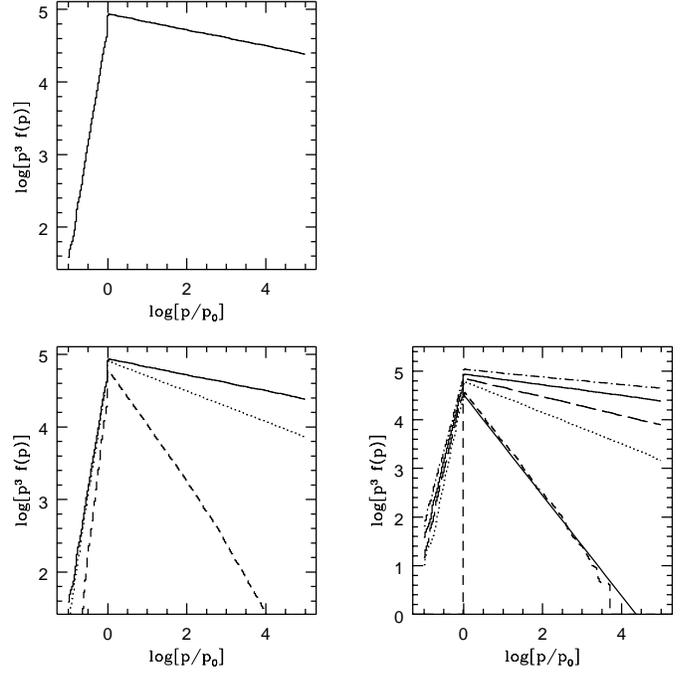


**Fig. 5a–c.** Differential logarithm spectrum produced by an ensemble of identical shocks. *Upper left panel* **a**: our refering case with $\tilde{t}_M/\tilde{t}_{esc} \sim 0.1$ (see text for parameters). *Lower left panel* **b**: the case with different escape times, in solid line $\tilde{t}_{\mathrm{esc}} = 1000$, in dotted line $\tilde{t}_{\mathrm{esc}} = 500$, and in short-dashed line $\tilde{t}_{\mathrm{esc}} = 100$. *Lower right panel* **c**: the case of different inter-shock distances, from the upper to the lower curve we have dashed-dotted line $L = 10$, solid line $L = 20$ our fiducial case, long-dashed line $L = 50$, dotted line $L = 100$, short-dashed line $L = 10^4$. The power-law spectrum corresponds to the single shock solution.

may in fact remain adequate. For low momentum $p \leq 1$, the spectrum steepens with decreasing $L$ and tends to $p^0$.

### 4.2. Multiple shock effect: the case with synchrotron losses

The stationary spectrum computed with the fiducial parameters is given in Fig. 6a. The inclusion of losses creates a pile-up at a momentum where losses equal gains i.e., $\tilde{t}_{\mathrm{M}} = \tilde{t}_{\mathrm{syn}}$. From the simulation, we find this occurs at roughly $\tilde{p} = 10^3$, which implies $\tilde{t}_{\mathrm{M}} \approx 100$ close to $5 \times \tilde{t}_{\mathrm{adv}}$. This provides an independent check on the estimate made from the results presented in Figs. 5b and 5c. The width of this hump on the low momentum side is determined by the momentum at which $\tilde{t}_{\mathrm{esc}} = \tilde{t}_{\mathrm{syn}}$, where escape intervenes to overwhelm the effects of synchrotron losses. Since $\tilde{t}_{\mathrm{esc}} = 50\tilde{t}_{\mathrm{adv}} \approx 10\tilde{t}_{\mathrm{M}}$, the hump makes its appearance about one order of magnitude before it peaks.

At momenta higher than the peak of the hump, the losses dominate over all other processes, since there $\tilde{t}_{\mathrm{syn}} < \tilde{t}_{\mathrm{adv}} \leq \tilde{t}_{\mathrm{M}}$, and, in this example, the acceleration at a single shock is approximately equal to the advection time (see Eq. 26). Consequently, the spectrum cuts off exponentially. This conclusion is consistent with the results of Melrose & Crouch (1997) found using an iterative method in which the synchrotron cut-off is estimated in advance.
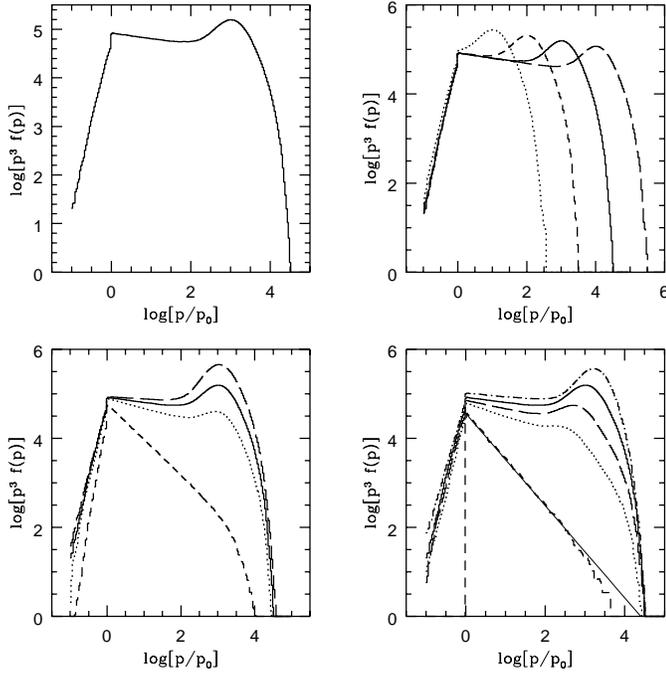
**Fig. 6a–d.** Differential logarithm spectrum for multiple shock acceleration with synchrotron losses. *Upper left panel* **a** our fiducial case, see text for the parameters. *Upper right panel* **b**: the case with different synchrotron loss rates, the solid line corresponds to our refering case, the short dashed and dotted lines have a loss rate divided by 10 and 100, and the long dashed has a loss rate multiplied by 10. *Lower left panel* **c**: the case with different escape time, from the upper to lower curve: $\tilde{t}_{\rm esc} = 210^3$, $10^3$ our refering case, 500, and 100. *Lower right panel* **d**: the case with different inter-shock distances, the distribution corresponding to our refering value $L = 20$ is in solid line. In dotted-dashed line $L = 10$, in long-dashed line $L = 50$, in dotted line $L = 100$, in short-dashed line $L = 10^4$. The power-law spectrum corresponds to the single shock solution with $\tilde{t}_{\rm S}/\tilde{t}_{\rm esc} \sim 210^{-2}$.

### 4.2.1. Variations of the loss rate

A decrease (increase) of $\tilde{a}_{\rm s}$ with $L$ and $\tilde{t}_{\rm esc}$ kept unchanged, leads to stronger (weaker) losses, and lower (higher) momenta at the peak of the pile-up. This is confirmed in Fig. 6b, which also demonstrates that the peak momentum is directly proportional to the loss time $\tilde{t}_{\rm syn}$. The width of the hump is unaffected, since its lower bound also moves in proportion to $\tilde{t}_{\rm syn}$. Radiative losses are unimportant below the injection momentum, except when the loss rate is so strong ($\tilde{a}_{\rm s} \sim 1$) that particle are prevented from being accelerated at all.

### 4.2.2. Effects of the other parameters

We stress here the effects of both escape and adiabatic losses on the shape of the pile-up.

– Keeping the inter-shock distance $L \equiv \tilde{t}_{\rm adv}$ constant and allowing $\tilde{t}_{\rm esc}$ to vary causes a change in both the spectral slope at low momenta, where losses are unimportant, and a change in the width of the pile-up Fig. 6c. As $\tilde{t}_{\rm esc}$ increases, the low momentum spectrum hardens, and the width of the hump in-

creases, as it shortens, the spectrum softens, and the hump becomes less prominent, until it disappears completely once $\tilde{t}_{\rm esc} < \tilde{t}_{\rm adv}$. At this point, the power-law index of the low momentum spectrum is approximately 4, in agreement with the findings of Kardashev (1962).

– Keeping the escape time constant, but varying the advection time (and inter-shock distance) enables one to distinguish the regimes of single and multiple shock acceleration. For larger values of $\tilde{t}_{\rm adv}$, than our fiducial case, four regions in momentum space can be found. Starting at low momentum, these are (Fig. 6d)

1. For $\tilde{t}_{\rm syn} > \tilde{t}_{\rm esc}$, acceleration proceeds by the multiple shock process without losses.
2. For $\tilde{t}_{\rm esc} > \tilde{t}_{\rm syn} > \tilde{t}_{\rm adv}$ the spectrum is affected by losses, and starts to form a pile-up. Acceleration at multiple shocks takes place.
3. For $\tilde{t}_{\rm adv} > \tilde{t}_{\rm syn} > \tilde{t}_{\rm S}$ particles are prevented from reaching the next shock before cooling. An interesting phenomenon appears in this case: the spectrum shows a power-law index appropriate to acceleration at a single shock front (see the dotted line)
4. For $\tilde{t}_{\rm S} > \tilde{t}_{\rm syn}$ losses dominate over all other processes and the spectrum cuts off.

In Fig. 6d all four regions can be distinguished in the case $L = 100$. At higher $L$, escape prevents multiple shock acceleration, and at lower values the shocks are too close together to allow the emergence of the single-shock power-law spectrum. These effects do not appear in previous works, which had to assume a separation in the time-scales of the different. The high momentum power-law tail due to the single shock process may be important and contribute a substantial fraction of the total pattern luminosity.

### 4.3. Synchrotron spectrum

The optically thin synchrotron emission produced by the particle distribution within a shock pattern described by Fig. 4, assuming constant magnetic field (i.e., parallel shocks) is given by

$$S_\nu \propto \int_{\tilde{p}_{\min}}^{\tilde{p}_{\max}} \int_{-L/2}^{L/2} \tilde{P}(\nu, p) f(\tilde{p}, \tilde{x}) \tilde{p}^2 \mathrm{d}\tilde{p}\mathrm{d}\tilde{x}. \tag{28}$$

where, for a relativistic particle of charge $q$, mass $m$, and pitch-angle $\vartheta$,

$$\tilde{P}(\nu, p) = \left(\frac{\sqrt{3}}{2\pi}\right) \frac{q^3 B \sin \vartheta}{mc^2} \frac{\nu}{\nu_c} \int_{\nu/\nu_c}^{\infty} K_{5/3}(\xi)\mathrm{d}\xi. \tag{29}$$

The characteristic frequency depends on $p$ as $\nu_{\rm c}(p) = 3\omega_{\rm c} \sin \vartheta\, p^2/(2m^2c^2)$, where the cyclotron frequency is $\omega_{\rm c} = qB/mc$. The integration over the particle position is done by computing the number of particles at a given momentum $p$ at each time step inside the pattern. This gives the quantity $N(\tilde{p}) = \int_{-L/2}^{L/2} f(\tilde{p}, \tilde{x})\tilde{p}^2\mathrm{d}\tilde{p}$ contributing at a given frequency by the factor $\tilde{P}(\nu, p)$ to the synchrotron spectrum produced by the pattern. Fig. 7 shows the resulting synchrotron spectrum.
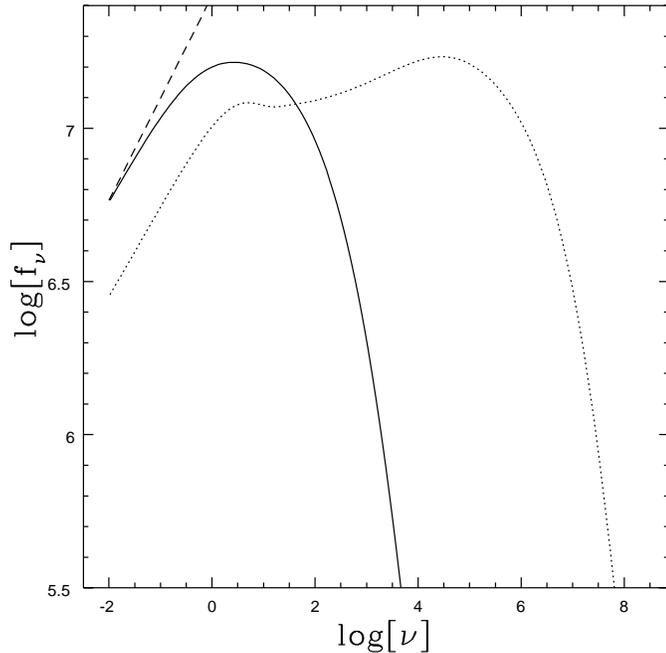
**Fig. 7.** Synchrotron spectrum produced by a periodic pattern. The solid lines line shows the synchrotron radiations produced if the loss rate is one hundred times stronger (see the solution in dotted line of Fig. 6b). We compare also the low momentum slope with a $1/3$ power-law spectrum is dashed line. The dotted line curve is produced for an escape time a factor two larger than in our refering case (see the solution in long-dashed curve of Fig. 6c).

The results, shown in Fig. 7, display a great variety of synchrotron spectra. For large ratios $t_{\rm esc}/t_{\rm adv}$ the spectrum is flat at low frequency, and extends over a range which depends on the relative strengths of loss and acceleration, which can be quite sufficient to explain the flat radio spectra observed in radio-loud quasars. Such an explanation provides an alternative to the inhomogeneous self-absorbed models usually advanced as the origin of flat radio Quasar spectra (Marscher & Gear 1985). Fig. 7 also shows that inverted spectra over 2–3 decades are also quite possible, where the cooling time is still shorter than the escape time. In fact the pile-up effect, as stressed by Melrose (1996), is essential to explain the inverted spectra observed in galactic centre sources such as Sagittarus $A^*$ (Beckert et al. 1996), and also may be associated with the flaring states of some extragalactic sources, such as the recent X-ray bursts of Mrk 501 (Pian et al. 1998). Such flares can arise from a variation of either the inter-shock distance or the escape time from the system. A change in the magnetic field stength does not mimick the multi-wavelength behaviour adequately (Mastichiadis & Kirk 1997).

## 5. Conclusions and outlook

Achterberg & Krülls (1992) and Krülls & Achterberg (1994, KA94) have demonstrated the usefulness of the stochastic differential equation approach as an efficient tool for investigating particle acceleration at shock fronts. They found approximate solutions of the diffusion-advection equations in several different physical situations including second order Fermi acceleration and momentum dependent spatial diffusion coefficients. However, their computational approach is limited to spatially resolved shock structures, and needs unrealistically short time steps for thin shocks. We have presented an improved scheme in which the particle momentum gain during a time step depends on both the initial and final positions of the particle. The scheme reproduces analytical results derived for shock thicknesses much lower than a typical diffusive length, without imposing an excessive requirement on the time step. We have applied our procedure to a system of multiple identical shocks. The $p^{-3}$ signature is obtained when the escape time is much larger than the multiple shock acceleration time. Inclusion of losses leads to a pile-up effect where the acceleration and loss rates are equal, as has been found analytically. The pile-up is present only for a restricted range of parameters: when the escape time exceeds the time for the plasma to move from one shock to the next, but is short enough not to permit synchrotron cooling of the lowest energy particles. We have shown that parameter ranges can be found in which the spectrum simultaneously displays the power law index characteristic of multiple shock acceleration (at low momenta) and the index appropriate to single shock acceleration at high momenta.

The synchrotron spectrum produced in each flow pattern can show flat or inverted spectra depending on the inter-shock distance, the loss strength and the ratio of escape to acceleration time. Multiple shock acceleration may explain the radio spectrum from flat radio Quasars, the radio to IR spectrum of galactic sources such as Sagittarus $A^*$, and even hard X-ray spectra observed in high states of the BL Lac Markarian 501.

Several extensions of this work are possible, such as the consideration of non-periodic flows and non-stationary injection. It also seems feasible to extend the 1D simulations to more complex multi-dimensional flows, such as numerical simulations of jets.

## References

Achterberg A., 1990, A&A 231, 251
Achterberg A., Krülls W.M., 1992, A&A 265, L13
Beckert T., Duschl W.J., Mezger P.G., Zylka R., 1996, A&A 307, 450
Blandford R.D., Ostriker J.P., 1980, ApJ 237, 793
Chalov S.V., Fahr H.J., Izmodenov V., 1995, A&A 304, 609
Conway A. J., MacKinnon A.L., Brown J.C., McArthur G., 1998, A&A 331, 1103
Drury L.O'C., Duffy P., Eichler D., Mastichiadis A., 1999, submitted to A&A
Gardiner C. W., 1983, Handbook of Stochastic Methods. Springer-Verlag, Berlin
Itô K., 1951, Mem. Am. Math. Soc. 4, 1
Ellison D.C., Jones F.C., Reynolds S.P., 1990, ApJ 360, 702
Jones F.C., Ellison D.C., 1991, Space Sci. Rev. 58, 259
Kardashev N.S., 1962, Sov. Astron. J. 6, 317

Kirk J.G., Melrose D.B., Priest E.R., 1994, In: Benz A.O., Courvoisier T.J.-L. (eds.) Plasma Astrophysics. Saas-Fee Advanced Course 24, Springer-Verlag, Berlin

Klöden P.E., Platen E., 1992, Numerical solutions of stochastic differential equations. Springer Verlag, Berlin

Krülls W.M., Achterberg A., 1994, A&A 286, 314 (KA94)

Lagage P.O., Cesarsky C.J., 1981, Proc. Int. School and Workshop on Plasma Astrophysics. Varenna, ESA-SP-161, 317

MacKinnon A.L., Craig I.J.D., 1991, A&A 251, 693

Marscher A.P., Gear W.K., 1985, ApJ 298, 114

Mastichiadis A., Kirk J.G., 1997, A&A 320, 19

Melrose D.B., 1996, In: Ekers R.D., Fanti C., Padrielli L. (eds.) Proceedings of the 175th symposium of the international astronomical union, Bologna, Italy. Kluwer Academic Publishers

Melrose D.B., Crouch A., 1997, PASA 14, 251

Pian E., et al., 1998, ApJ 492, L17

Pope M.H., Melrose D.B., 1993, PASP 11, 175

Protheroe R.J., Stanev T., 1999, Aph 10, 185

Schlickeiser R., 1984, A&A 136, 227

Schlickeiser R., 1989, ApJ 336, 264

Schneider P., Kirk J.G., 1987, ApJ 323, L87

Schneider P., 1993, A&A 278, 315

Skilling J., 1975, MNRAS 172, 557

Smith A.M., Gardiner C.W., 1989, Phys. Rev. A39, 3511

Spruit H.C., 1988, A&A 319, 194

Webb G.M., Drury L.O'C., Bierman P., 1984, A&A 137, 185